A Bicyclic P–P-Bridged 1,3,2,4-Diphosphadiboretane Cation and an Imino(phosphinidene)borane–$AlBr_3$ Adduct[‡]

Klaus Knabel,[a] Thomas M. Klapötke,[a] Heinrich Nöth,*[a] Robert T. Paine,[b] and Ingo Schwab[a]

Dedicated to Prof. Dr. Alfred Schmidpeter on the occasion of his 70th birthday

Keywords: 1,3-Di(*tert*-butyl)-2,4-bis(2,2,6,6-tetramethylpiperidino)-1,3,2,4-diphosphadiboretane / 1-*tert*-Butyl-2,4-bis(2,2,6,6-tetramethylpiperidino)-1,3-diphospha-2,4-diborabicyclo[1.1.0]butane cation / 2,2,6,6-Tetramethylpiperidino-*tert*-butylphosphinideneborane–$AlBr_3$ adduct / X-ray structures / ab initio calculations

Depending on reaction conditions the 1,3,2,4-diphosphadiboretane **1** reacts with $AlBr_3$ to give the unstable adduct tmp=B=P(*t*Bu)$AlBr_3$, **3**, and/or the somewhat more stable salt $[(tmpB)_2(PtBu)P]^+[AlBr_4]$, **2**. The X-ray structure determination of **3** shows an almost linear NBP array with BN and BP double bonds resembling an allene type structure. NBO analysis shows the presence of BN- and BP-π-bonds. On the other hand, the cation of compound **2** has a bicyclic structure with a long P–P bond [2.349(2) Å]. The B–P bonds to the phosphonium type P2 atom [av. 1.939(5) Å] are longer than those to the tri-coordinated P1 atom [1.889(6) Å]. NBO analysis of the model compound $(H_2NB)_2(PMe)P^+$, **9**, show that the P–P bond in **2** is formed from *p*-orbitals.

Introduction

In contrast to boron nitrogen chemistry, the development of the chemistry of B–P compounds began much later, but has attracted increasing attention during the last two decades. The state of the art has been summarized in a review.[2] Particularly 1,3,2,4-diphosphadiboretanes[3–11] offer many interesting aspects as ligands as well as a source for amino-phosphinidene-boranes $R_2N{=}B{=}PR$[8,11] having a boron atom of coordination number 2 and B=N as well as B=P double bonds. They also react with many Lewis acids often in rather unusual ways,[12] and we report here on the reaction of $[tmpB\text{-}PtBu]_2$, **1**, (tmp = 2,2,6,6-tetramethylpiperidino) with $AlBr_3$.

Results

Synthesis and Reactions

The chemistry of 1,3,2,4-diphosphadiboretanes is well developed. Many derivatives have been synthesized, characterized, and their chemistry studied to some extent.[2] For example, in most cases reactions with metal carbonyl fragments lead simply to coordination of the P atoms of the intact four-membered ring.[6,7] More interesting are reactions where cycloreversion produces phosphinidene boranes with dicoordinated B atoms as shown for $(tmpB\text{-}PCEt_3)_2$,[11] which gives the complex tmp=B=PR–$Cr(CO)_5$.[5] This suggests that other Lewis acidic compounds or fragments might behave similarly. Another ideal candidate for cycloreversion reactivity is the diphosphadiboretane $(tmpB\text{-}PtBu)_2$, **1**. The synthesis of this compound has already been reported.[4] We now find that the reaction sequence Equation (1) allows the synthesis of **1** in a one pot reaction with yields of up to 81%.

The subsequent reaction of **1** with $AlBr_3$ in a 1:2 ratio in toluene solution at room temperature proceeds unexpectedly by P–C bond cleavage, according to Equation (2), to give compound **2**, which crystallized from toluene at –30 °C as yellow prisms. The compound is stable for more than a week in toluene below –20 °C. However, compound **2** is not the primary reaction product. Monitoring the reaction by ^{31}P and ^{11}B NMR spectroscopy at –30 °C we find that the primary reaction leads to the yellow 1:1 adduct tmp=B=P*t*Bu·$AlBr_3$, **3**, on rapid addition of an excess of $AlBr_3$ to **1** (ratio 2:1) as shown in Equation (3). Compound **3** quickly converts, at room temperature, from a solid into an orange oil which finally yields the golden yellow compound **2** after addition of toluene. At low temperatures (below –20 °C) both **2** and **3** are stable for some hours in tolu-

[‡] Contribution to the Chemistry of Boron, 255. Part 254: Ref.[1]

[a] Department of Chemistry, University of Munich, Butenandtstr. 5–13, 81377 München, Germany
[b] Department of Chemistry, University of New Mexico, Albuquerque, NM 87131, USA

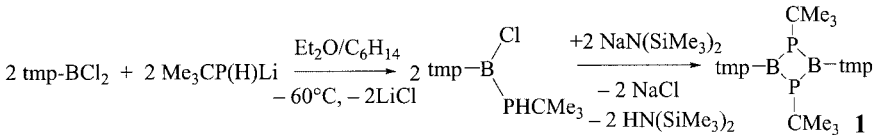

(1)

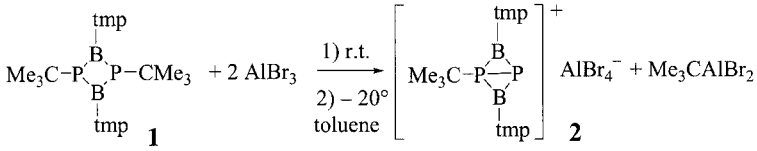

(2)

ene. In the solution of **2** the formation of tBuAlBr$_2$ was detected by its ^{27}Al NMR signal at δ = 152.5 ppm. Compound **2** is nearly insoluble in pentane but reacts with $CDCl_3$ and more slowly in CD_2Cl_2 solution.

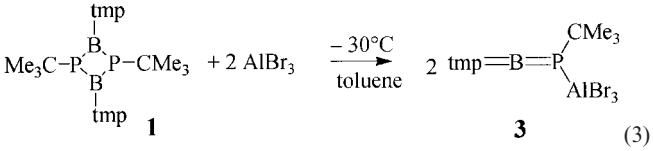

(3)

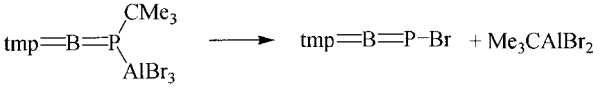

(4)

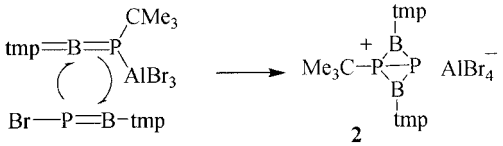

(5)

There are at least two conceivable mechanisms for the formation of the salt **2**. We prefer the one that is shown in Equation (4) and Equation (5) as **3** is one of the isolated products, i.e. we assume a decomposition of **3** with elimination of tBuAlBr$_2$ [Equation (4)] and cycloaddition of the proposed intermediate BrP=Btmp with **3** [Equation (5)].

The reaction of **1** with $AlCl_3$ in toluene produced a yellow powder that was insoluble in nonpolar solvents. Elemental analyses of products from several experiments ranged from 6.74 to 8.38% for Al, and from 29.80 to 34.70% for Cl. These data show that the Cl:Al ratio is close to 3. However, IR data are not conclusive as to whether the product is an analogue of **2** or **3** or something else**.** With $GaCl_3$ the same observation was made for toluene solutions. The colorless powder which forms decomposes at about 185°C. The ^{11}B NMR spectrum of the solution showed the presence of tmpBCl$_2$ (δ^{11}B = 33.8 ppm) besides a signal at δ^{11}B = 44.5 ppm. In the ^{31}P NMR spectrum of the $GaCl_3$ reaction five signals are observed at –181.4 [d, $J(^1H^{31}P)$= 110 Hz], –148.7 [d, $J(^1H^{31}P)$= 110 Hz], 91.9, 7.9, and 1.8 ppm, indicating that no single species is present in solution. In contrast, $InCl_3$ in the toluene suspension did not react at all with **1**. This demonstrates the unique behavior of $AlBr_3$.

NMR Spectra

The rapid decomposition of **3** made the recording and interpretation of the NMR spectra difficult, particularly for the ^{1}H and ^{13}C NMR spectra due to the presence of **2** and other by-products.

It is surprising to note that the shielding of the ^{11}B nucleus in **3** is only 4.6 ppm, less than in the starting diphosphadiboretane **1** in spite of the fact that the boron atom is now dicoordinate. However, in agreement with this, the line width has increased from 400 (for, **1**) to 530 Hz for **3**. The small amount of deshielding is most likely due to the presence of BN- and weaker BP-π-bonding which leads to a comparatively high electron density at the boron atom (see results of calculations). Moreover, the δ^{11}B value is very close to those of tmp=B=P(tBu)M(CO)$_5$ (M = Cr, W)[5] which are 67.0 and 62.9 ppm. The ^{31}P NMR signal of **3** is broad ($h_{1/2}$ = 900 Hz) and found at δ = –59.8 ppm. This P atom environment is better shielded than in the M(CO)$_5$ complexes (δ^{31}P = –32.7 and –45.3 ppm for M = Cr and W, respectively). Its ^{27}Al NMR spectrum contains a doublet at δ = 98.3 ppm due to AlP coupling with $^1J(^{31}P^{27}Al)$ = 140 Hz. The small line width of 20 Hz, as well as the chemical shift, is typical of a tetracoordinate Al atom.

Due to the low solubility the ^{13}C NMR spectroscopic data of **3** could not be recorded in deuterated benzene. Reliable assignment of the ^{1}H NMR spectrum was also not possible. Similarly, the very low solubility of **2** in deuterobenzene or deuterotoluene resulted in the detection of ^{1}H NMR resonances only for the *tert*-butyl group. In $CDCl_3$ rapid decomposition of **2** occurred. In CD_2Cl_2 the decomposition was slow enough to allow the measurement of several NMR resonances. Nevertheless, even under these circumstances the compound decomposed completely within 15 to 20 min. Thus, the measurements had to be done very quickly with as few pulses as possible. For this reason we were unable to get ^{13}C NMR spectroscopic data of compound **2**, and only the ^{1}H resonance for the tBu group could be reliably assigned as a doublet due to $^3J(^{31}P^1H)$ = 11 Hz.

The boron atoms in the cation of **2** are more shielded by 30 ppm compared with **3.** As expected, the line width is much smaller (280 Hz) since the B atoms are tricoordinate. The observed two ^{31}P signals were doublets with $^{1}J(^{31}P^{31}P)$ = 62 Hz in accordance with the calculations, and the shift difference of 40 ppm is 6 ppm from the calculated value.[13] The small coupling constant suggests that the bond between the two P atoms does not represent a normal P–P single bond as found e.g. in 3-(diisopropylamino)-4-(dimethylamino)-1,2-di(*tert*-butyl)-1,2,3,4-diphosphadiboretane.[14] The presence of the tetrabromoaluminate anion in **2** is manifested by a sharp ^{27}Al NMR signal at δ = 80.3 ppm.[15]

The IR spectrum of **3** is characterized by two strong bands at 1633 and 1590 cm^{-1}. These heteroallene bands are 26 and 23 cm^{-1} higher than those observed for tmp=B=P(*t*Bu)M(CO)$_5$[5] indicating stronger BN and BP bonds. In tmp=B=N(*t*Bu)$AlBr_3$ these bands are found at 1800 and 1850 cm^{-1}.[16] This is due to a better coupling of the two BN vibrations, and obviously stronger BN bonds.

The mass spectrum of **3** shows few peaks, and there is no peak for the molecular ion. The most intense peak is found at *m*/*z* = 298. It can be assigned to the $PAlBr_3$ fragment due to the isotopic pattern. A peak at *m*/*z* = 426 (22%) results from loss of a Br atom from the molecular ion. Loss of a Me group from this ion, either from the *t*Bu group or the tmp substituent, leads to a peak at *m*/*z* = 411 (35%).

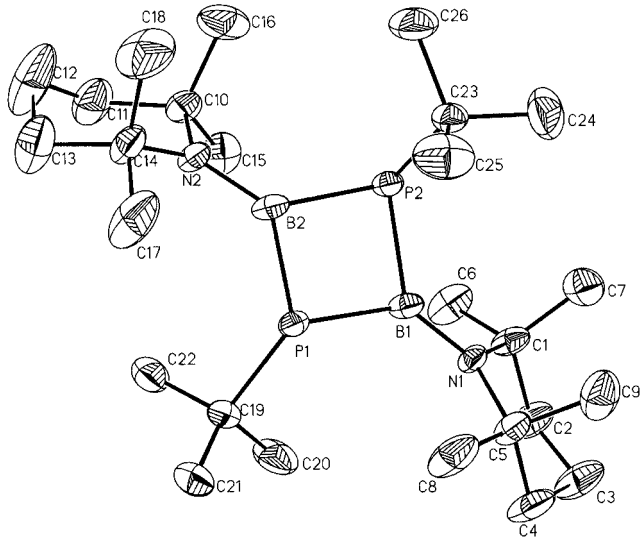

Figure 1. The molecular structure of **1** in ORTEP description. Thermal ellipsoids are represented on a 25% probability level. Selected bond lengths (Å): P1–B1 1.876(9), P1–B2 1.865(6), P1–C19 1.895(7), P2–B2 1.943(8), P2–B1 1.948(6), P2–C23 1.880(7), B1–N1 1.408(8), B2–N2 1.419(8), N1–C1 1.503(7), N1–C5 1.492(7), N2–C10 1.494(8), N2–C14 1.492(7). Selected bond angles (°): B1–P1–B2 90.1(3), B1–P1–C19 124.1(3), B2–P1–C19 124.9(3), B1–P2–B2 85.9(3), B1–P2–C23 111.1(3), B2–P2–C23 112.1(3), N1–B1–P1 134.7(5), N1–B1–P2 133.5(6), P1–B1–P2 91.6(3), P1–B2–P2 92.1(3), N2–B2–P2 133.3(5), N2–B2–P1 134.4(6), B1–N1–C1 118.5(5), B1–N1–C5 122.8(5), C1–N1–C5 118.4(5), B1–N2–C10 118.5(5), B2–N2–C14 143.8(5), C10–N2–C14 118.1(5).

Molecular Structures

Figure 1 shows the molecular structure of the diphosphadiboretane **1**. The compound crystallizes in orange prisms in the monoclinic system, space group $P2_1/c$ with Z = 4. The four-membered ring is asymmetric with unequal B–P bond lengths spanning a range from 1.865(6) to 1.948(6) Å. This results in endocyclic bond angles also being different with P–B–P angles of 91.6(2)° at B1 and 92.1(3)° at B2 and B–P–B bond angles of 90.1(3)° at P1, and 85.9(3)° at P2. As expected, the B and N atoms reside in planar environments, e.g. the sum of bond angles for N1 is 359.7°, and 359.8° for N2. The B–N bonds are on the upper end of the range of B(sp^2)–N(sp^2) bonds in monoaminoboranes. The reason for this is that the tmp groups are twisted against the respective P_2B planes by 47.8° for the C1N1C5 plane and by 51.1° for the C10N2C14 plane. This twisting is due to steric repulsion of the bulky organyl groups. Actually, the BN bond lengths found for **1** are intermediate with those determined for (tmpB-$PCEt_3$)$_2$ (1.431 Å)[11] and (tmpB-$PH)_2$ (1.405 Å).[7] In contrast to most other 1,3,2,4-diphosphadiboretanes, the four-membered ring of **1** is not planar whereas calculations (v. i.) predict a planar ring structure: the two P_2B planes are bent by 7.1° (roof angle 172.9°). The angle that the PC bonds form with their respective P_2 bonds are also unusual: for P2–P1–C19 this angle is 149.7° while an angle of 126.7° is found for P2–P1–C23.

The molecular structure of **3** is depicted in Figure 2. This compound also crystallizes in the monoclinic system, space group $P2_1/n$ with Z = 4. The molecule is characterized by a dicoordinated B atom and by tricoordinate N and P atoms. The plane C1N1C5 lies almost perpendicular to the plane Al1P1C10 as expected for an allene type configuration. This is in agreement with an N–B–P bond angle of 170.4(3)°. Similar deviation from the ideal linearity has been observed for compounds of type tmp=B=N(*t*Bu)(Cr[CO)$_5$[16] or tmp=B=N(*t*Bu)ECl_3 (E = Ga, In).[17] While atom N1 sits in the center of the C1C5B1 plane, the sum of bond angles at atom P1 is only 334.4°. Thus, the geometry about the P1 atom is pyramidal. The bond angle C10–P1–Al1 is 118.2(2)° and the other two angles, B1–P1–C10 and B1–P1–Al1 are 110.6(2) and 105.6(2)°, respectively. This corresponds with a distorted trigonal pyramid. Consequently, this geometry is not optimal for BP-π-bonding. One can indeed note that the B–P bond length in **3** [1.787(4) Å] is somewhat longer than in tmp=B=P(*t*Bu)Cr(CO)$_5$[5] [1.742(5) Å] where the P atom resides in a planar environment. Nevertheless, the B–P bond length in **3** is shorter than expected for B–P single bonds for which a range from 1.81 to 1.91 Å has been determined in agreement with covalent radii and taking the Shoemaker–Stevenson correction into account.[18] It should be noted, however, that in most cases a covalent bond length increases as the coordination number of an atom decreases, thus the B–P bond in **3** can still be considered to have multiple bond characteristics. However it does not show the

geometry of a classical pp–π-bond in contrast to the model compound $Me_2N{=}B{=}P(Me)AlBr_3$ (**10**), see below.

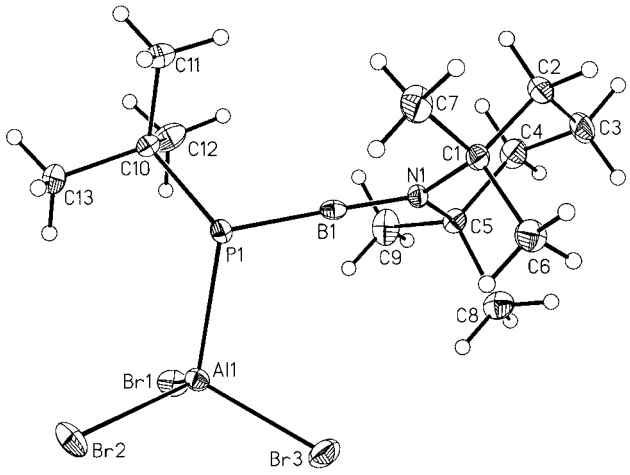

Figure 2. The molecular structure of **3** in ORTEP description. Thermal ellipsoids are shown on a 25% probability level. Selected bond lengths (Å): Al1–Br1 2.279(1), Al1–Br2 2.302(1). Al1–Br3 2.281(1), Al1–P1 2.67(1), P1–B1 1.787(4), P1–C10 1.892(3), N1–B1 1.331(4), N1–C1 1.529(4), N1–C5 1.527(4). Selected bond angles (°): Br1–Al1–Br2 109.40(4), Br1–Al1–Br3 112.49(4), Br1–Al1–P1 111.95(4), Br2–Al1–P1 107.66(5), Br3–Al1–P1 104.36(4), B1–P1–C10 110.6(2), B1–P1–Al1 105.6(1), Al1–P1–C10 118.2(1), N1–B1–P1 170.4(3), B1–N1–C1 119.5(3), B1–N1–C5 119.7(3), B1–N1–C5 120.7(2).

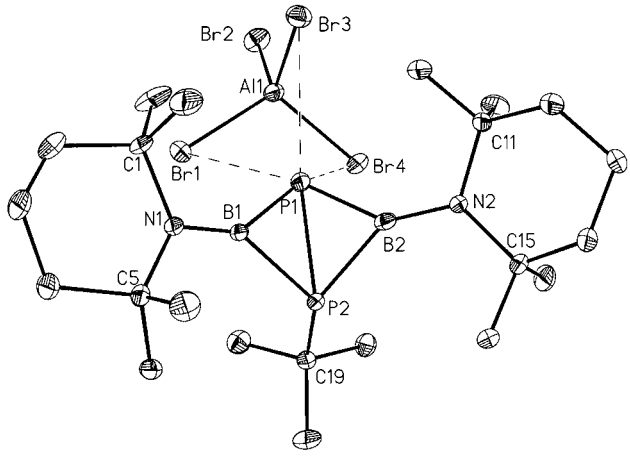

Figure 3. The molecular structure of **2** in ORTEP description. Thermal ellipsoids are depicted on a 25% probability level. Selected bond lengths (Å): Al1–Br1 2.310(2), Al1–Br2 2.293(2), Al1–Br3 2.297(2), Al1–Br4 2.308(2), P1–P2 2.315(2), P1–B1 1.894(6), P2–B1 1.944(5), P1–B2 1.884(7), P2–B2 1.931(6), B1–N1 1.360(6), B2–N2 1.377(8), N1–C1 1.532(6), N1–C5 1.534(6), N2–C10 1.537(6), N2–C14 1.519(6). Selected bond angles (°): B1–P1–B2 90.4(3), B2–P1–P2 53.6(2), B1–P1–P2 53.9(2), B1–P2–B2 87.6(2), B2–P2–P1 51.7(2), B1–P2–P1 51.9(2), B1–P2–C19 123.9(3), B2–P2–C19 124.6(2), N1–B1–P1 143.9(4), N1–B1–P2 141.9(4), P1–B1–P2 74.2(2), P1–B2–P2 74.7(2), N2–B2–P1 142.1(4), N2–P–B2–P2 142.9(4), B1–N1–C1 118.0(4), B1–N1–C5 121.8(4), C1–N1–C5 118.5(4), B2–N2–C10 118.3(4), B2–N2–C14 122.1(4), C10–N2–C14 118.8(4), P1–P2–C110.1(4).

The molecular structure of compound **2** is shown in Figure 3. The bicyclic ring has a butterfly configuration with the P atoms at the roof and an angle of 123.4° between the two P_2B planes. This fold angle differs enormously from that in **1** (172.9°), but corresponds with the bicyclo[1.1.0]-butane structure with a "roof" angle of 126°.[19] The B and N atoms of **2** have a planar environment, demonstrating their sp^2 type character which allows good BN-π-bonding. This is not only shown by short BN bonds [1.360(6) Å for B1–N1, and 1.377(8) Å for B2–N2] but also by the fact that the torsion angles τ of C1–N1–B1–P1 and C14–N2–B2–P2 are only 16.3 and 15.4°, respectively.

The P–B bonds in the cation of **2** are shorter for P1 (1.894(6) and 1.884(7) Å) than those at atom P2 which show bond lengths of 1.944(5) and 1.931(6) Å. These longer bonds are in line with the higher coordination number at atom P2. Of particular interest is the P1–P2 distance, 2.315(2) Å. This is longer than the usual P–P single bond length, 2.15(2) Å, but compared with the PP separation in the related diphosphadiboretane (tmpB-P*t*Bu)$_2$, **1**, there is a shortening by 0.427 Å. This is consistent with the presence of a weak P–P bond in **2**. The two B–P–B bond angles are close to 90° [90.4(3)° for P1 and 87.6(2)° for P2]. On the other hand, we find the P–B–P bond angle at B1 to be 74.2(2)°, and 74.7(2)° for B2, while the B1–P1–P2 and B2–P1–P2 angles are 53.9(2)° and 53.6(2)°.

Twhere is a very weak interaction of atom P1 with the bromine atom Br3 of the tetrabromoaluminate anion (P1···Br3 3.720 Å). The other two "contacts", P1···Br1 and P1···Br4 show distances of 3.965 and 4.166 Å, respectively. The Al–Br bonds lie in the range of 2.293 to 2.310 Å and the Br–Al–Br bond angles range from 108.6 to 110.1°. The Br3···P1 interaction has no elongating effect on the Al1–Br3 bond (Al1–Br3 2.297 Å).

Theoretical Studies

The formation of the $(tmpB)_2P_2tBu^+$ cation in **2** is not only unusual but also of interest considering bonding situation and structure. Therefore, we performed ab initio and density functional calculations at various levels not only for the gas phase structure of compound **2** but also for the model compounds **5** to **10**, **5** being a model for the cation in compound **2**. Moreover, ELF calculations were performed for the model compounds **9** and **10** (see Figures 7 and 8, molecule **8** is not depicted but calculations have been performed for comparison).

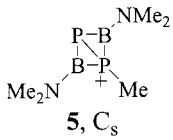

5, C_s

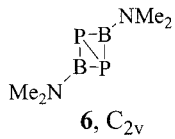

6, C_{2v}

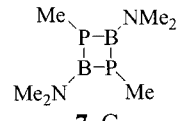

7, C_1

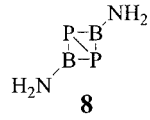

8

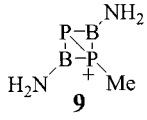

9

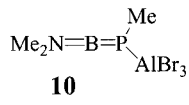

10

Compound **1** is an analogue of **7**. While **1** has a slightly bent ring structure and shows two differently *trans*-oriented P–C bonds with respect to the P1/P2 atoms, the calculations for model **7** in the *trans*-configuration reveal a planar ring structure with longer P–B bonds, and, more noticeably, the P–B–P bond angle is 8° larger than that calculated for the *cis*-isomer of **7** (see Figure 4). Compound **1** has only been observed as the *trans*-isomer which is obviously the more stable structure, and this has been ascertained for *cis*-**7** which is 611.6 kJ/mol less stable than the *trans*-isomer. Figure 5 shows the results of the calculations for the *trans*-isomer.

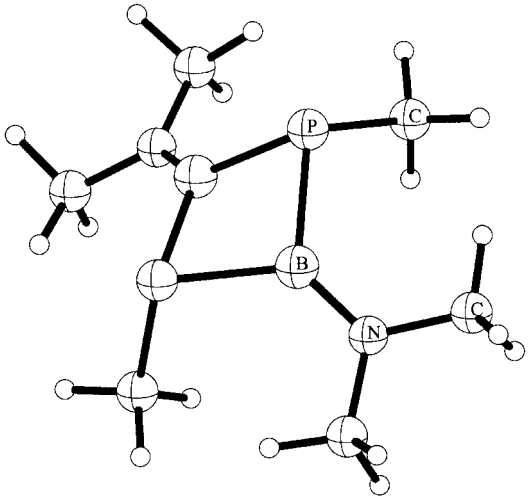

Figure 4. Optimized structure for the model compound *cis*-[$(Me_2B)_2$-$(PMe)_2$], **7** (C_{2v}) at the RI-MP2/TZVP level of theory. Bond lengths (Å) and angles (°): P–B 1.943, P–C 1.885, B–N 1.399*N*–C 1.455; P–B–P 98.60, B–P–B 74.15, B–P–C 106.51, P–B–N 130.67, B–N–C 123.71; torsion angle P–B–B–P 143.9.

Table 1 contains calculated data for compound **6** and experimental data for compound **4**, respectively. It also shows selected experimental and calculated data for the cation in compound **2** as well as calculated values for the model **5**

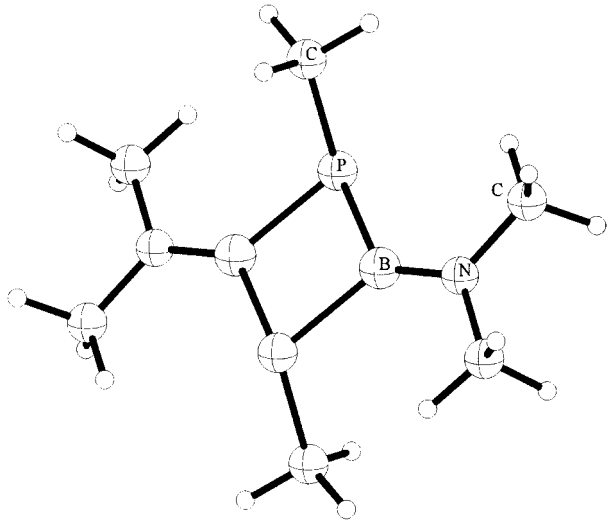

Figure 5. Optimized structure for the model compound *trans*-[$(Me_2B)_2(PMe)_2$], **7** (C_1) at the RI-MP2/TZVP level of theory. Bond lengths (Å) and angles (°): P–N 1.924, P–C 1.875, B–N 1.395, N–C 1.452; P–B–P 97.95, B–P–B 82.05, B–P–C 114.26, P–B–N 131.03, B–N–C 123.28; torsion angle 0.01.

(C_1 and C_s; see also Figure 6). It also contains experimental and calculated ^{31}P chemical shifts. The ^{31}P spectrum of the cation of **2** showed two doublets with $^1J(^{31}P^{31}P)$ = 62 Hz and a separation of the two signals by 40 ppm. These data are roughly in agreement with the calculated values for the model cation **5** with C_1 or C_s symmetry. The largest deviation between experimental and calculated data results for the bond angle P1–P2–C, most likely a result of the different steric requirements of the tmp and Me_2N groups.

Selected data from the NBO analysis of **9** and **10** are listed in Table 2 and Table 3. It is noteworthy that the P–P bond in **9** is built almost exclusively from the *p*-orbitals of the phosphorus atoms. While the P1–B bond results from a boron sp^2 and a phosphorus *p*-orbital (86% p character),

Table 1. Experimental parameters from X-ray diffraction and ^{31}P NMR shifts for compounds **2** and **4** together with the calculated parameters of the cation of **2** and the model compounds **5** and **8**.

Compound	**4**	**6** (C_{2v})		**2**	**2** calcd. (C_1)		**5** (C_s)	
Method	exp.	RI-MP2 [a]	RI–CC2	exp.	RI–BP86	RI-MP2/SV(P)	RI-MP2	RI–CC2
P1–P2	2.349(2)	2.459	2.465	2.315(2)	2.331	2.328	2.385	2.393
P1–B	1.904(6)/1.907(5)	1.898	1.901	1.884(7)/1.894(6)	1.908/1.911	1.897/1.901	1.890	1.891
P2–B	–	–	–	1.931(6)/1.944(5)	1.947/1.955	1.925/1.932	1.925	1.926
B–N	1.385(7)/1.381(9)	1.390	1.395	1.360(6)/1.377(8)	1.386/1.387	1.381/1.382	1.366	1.372
N–C	1.528(7)/ 1.525(7)	1.455	1.456	1.519(6)–1.537(6)	1.535–1.546	1.517–1.524	1.466	1.470
P2–C	–	–	–	1.884(5)	1.943	1.892	1.846	1.850
B–P–P	51.9(1)/52.0(1)	49.64	49.58	90.4(3)	51.97/53.82	51.86/52.05	50.66/51.97	50.56/51.80
P–B–P	76.0(2)/76.2(3)	80.73	80.84	74.2(2)/74.7(2)	74.21/74.34	74.89/74.96	77.37	77.63
P–B–N	141.4(1)/141.6(2)	139.51	139.48	87.6(2)	141.78–144.00	140.40–144.69	137.83/144.25	137.78/144.01
P1–P2–C	–	–	–	123.9(3)	111.32	109.41	110.42	110.58
B–P2–C	–	–	–	123.9(3)/124.6(2)	124.60/125.16	124.2/124.9	122.82	122.68
Roof angle	104.1	101.9	101.28	123.4	123.36	121.56	127.46	128.06
$\delta = {}^{31}P$[b]	–290 ppm [3]	–280 ppm		not reproducible	–121.6/187.6–ppm		–223/–257 ppm	

[a] TZVP basis sets used unless noted otherwise. [b] NMR shifts at the GIAO/MP2 level, except for [(tmpB)2(P*t*Bu)P]$^+$ (**2**) which has been calculated at the BP86 level because of exceedingly high memory requirements for MP2.

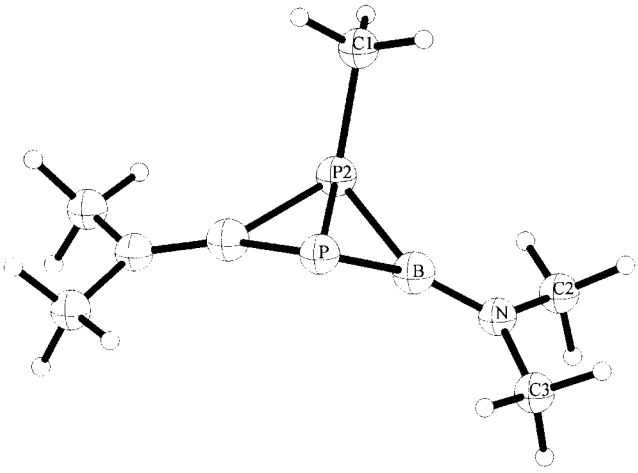

Figure 6. Optimized geometry (C_s) for the model cation **5** at the RI-MP2/TZVP level of theory. Bond lengths (Å) and angles (°): P–P2 2.385, P–B 1.890, P2–B 1.925, P2–C1 1.846, B–N 1.366, N–C2 1.466, N–C3 1.468; P–P2–B 50.66, P–B–P2 77.37, B–P–P2 51.97, P–P2–C1 110.42, P–B–N 137.83, B–N–C2 124.17, B–N–C3 122.13

the P2–B bond is formed from a boron sp^3 orbital and a phosphorus sp^2 orbital. The positive charge of the cation resides mainly on the tetracoordinate P atom (see data in Figure 6). As expected, the B–N bonds are double bonds.

A similar situation is present in the $AlBr_3$ adduct **10**. Both, the B–N and the B–P bonds are double bonds.

Finally, the bonding situation in **2** and **3** as calculated for the model compounds **9** and **10** is illustrated by the use of topological ELF analysis (electron localization function),[20] as depicted in Figure 7 and Figure 8, calculated for C_s and C_1 symmetry, respectively. There are four B–P bonds and a weak P–P bond that form the B_2P_2 core of **9**. The corresponding attractors are above the two BP_2 planes. The disynaptic basins of these attractors are merged in the case of the alkyl-substituted atoms P2. Regarding the location of positive charges: the tetracoordinate atom P2 carries a higher positive charge than atom P1, which is almost neutral, and as expected the boron atoms also carries a positive charge while negative charges are primarily located at the N atoms. Figure 8, on the other hand, clearly shows the allene type structure of the $AlBr_3$ adduct **10** (orthogonal attractor positions) and also reveals BN- and BP-π-bonding.

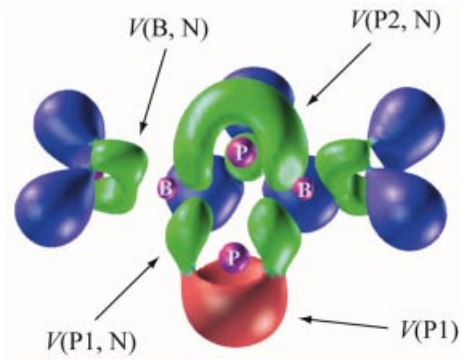

Figure 7. Rendered *ELF* isosurface and basin assignment for $[(H_2NB)_2(PMe]P)]^+$ (**9**C_s) with disynaptic basins (green) and monosynaptic basin *V*(P1) (red). Representation at η = 0.80, 150^3 grid points, core basins in purple, protonated basins in blue. The *V*(P1, P2) for the weak interaction between the two phosphorus atoms has a maximum *ELF* value of 0.645 and is therefore difficult to visualize. AIM basin populations (charges): P1 15.04 (–0.04), P2 14.76 (+0.24), B1/B2 3.89 (+1.11), N 8.54 (–1.54).

Discussion

1,3,2,4-Diphosphadiboretanes (RB–PR′)$_2$ are more readily accessible than the six-membered 1,3,5,2,4,6-triphosphatriboranes but need bulky groups R for stabilization. The 2,2,6,6-tetramethylpiperidino is such a group as shown e.g. by (tmpB-PH)$_2$.[17] Another one is the mesityl group

Table 2. Selected data from the NBO analysis of the model compound **8** at the MP2/TZVP level of theory, reflecting the bonding situation in **2.**

Bond	Degree of occupation	Bonding in % electrons		Share in % of AO′s	
P1–P2	1.66	P1: 41	P2: 59	P1:s 1 p 98 d 1	p2:s 2 p 97 d 1
P1–B	1.85	P: 53	B: 47	P:s 14 p 86	B:s 35 P 65
P2–B	1.87	P: 59	B: 41	P:s 33 p 67	B:s 25 p 75
B–N (σ)	1.97	N: 74	B: 26	N:s 48 p 52	B:s 40 p 60
B–N (π)	1.95	N: 81	B: 19	N:s 0 p 100	B:s 0 p 100
P–C	1.94	P: 45	C: 55	P:s 33 p 67	C:s 23 p 77

Table 3. Selected data from the NBO analysis of the model compound **10** at the MP2/TZVP level of theory, reflecting the bonding situation in **2**.

Bond	Type	Degree of occupation	Bonding in % electrons		Share in % of AO′s	
P–B	σ	1.97	P: 57	B: 42	P:s 33 p 67	B:s 51 p 49
P–B	π	1.93	P: 74	B: 26	P:s 3 p 97	B:s 7 P 93
B–N	σ	1.99	N: 79	B: 21	N:s 41 p 59	B:s 42 p 58
B–N	π	1.95	N: 82	B: 18	N:s 0 p 100	B:s 0 p 100
P–Al	π-donor	1.87	P: 81	Al: 19	P:s 35 p 65	Al:s 19 p 81
P–C	σ	1.97	P: 47	C: 53	P:s 29 p 71	C:s 22 p 78

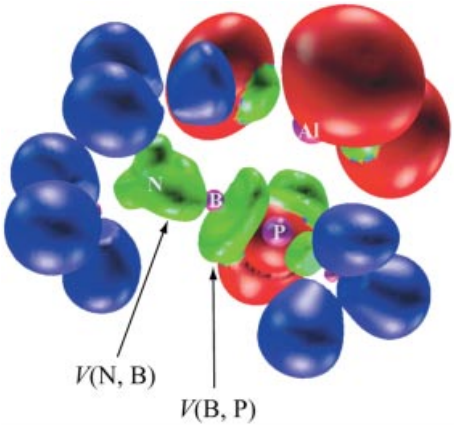

Figure 8. Rendered *ELF* isosurface and basin assignment for $AlBr_3$ adduct (**10**) with disynaptic basins (green). Representation at η = 0.75, grid increment 0.2 Å, core basins in purple, protonated basins in blue. The *ELF* surface illustrates the allene type character of the N–B–P moiety. Attractor distances (Å): P–*V*(P, Al)–Al: 1.026, 1.503; P–V(P, B)–B: 1.083, 0.775; P–V(P, C)–C: 1.024, 0.859; B–V(B, N)–N: 0.738/0.747, 0.701/0.718. AIM basin populations (charges): N 8.37 (–1.37), B 4.41 (+0.59), P 14.66 (+0.34), Al 11.02 (+1.98).

attached to the B atom.[21,22] Table 4 lists some typical structural features as well as ^{11}B and ^{31}P NMR spectroscopic data of some 2,4-diamino-1,3,2,4-diphosphadiboretanes. A more complete survey is given in a review.[2] A small range is observed for the B–P bond lengths (1.865 to 1.97 Å) which is typical for a B–P single bond between tricoordinate B and P atoms. In almost all cases the BN bonds are close to 1.4 Å with extremes of 1.37(1) to 1.431(2) Å. It appears that the B–P bond lengths are influenced by the steric requirements of the amino groups at the boron atoms: the smaller the amino group the longer is the B–P bond. This is coupled with the lengths of the B–N bonds and coplanarity of the C_2N plane with the BP_2 plane, e.g. the strength of the BN bond. Moreover, this also becomes apparent in the respective $\delta^{11}B$ values where deshielding is noted for the diphosphadiboretanes (tmpB-PR)$_2$ with an increasing steric demand of the R substituents (R = H, $\delta^{11}B$ = 47.1 ppm; R = CMe_3, $\delta^{11}B$ = 50.2 ppm; R = CEt_3,$\delta^{11}B$ = 66.1 ppm). Most of the four-membered rings are planar, and many of them show C_i point group symmetry. Therefore, the nonplanar rings of **1** as well as (tmpB-PSiMe$_3$)$_2$[4] are exceptional, particularly in comparison with the planar ring in (tmpB-PCEt$_3$)$_2$ where the P substituent is more bulky.[11] Nonplanarity is also observed for the two B_2P_2 rings of $Et_3CP(Btmp)_2P$–P(tmpB)$_2$PCEt$_3$,[23] whose angles between the P_2B planes are 157.2° within a bicyclic ring, and 98.4° between adjacent rings. The P–P bond length joining the two four-membered rings is 2.189(1) Å. In compound **4**, which results from the photolysis of (tmpB-PCEt$_3$)$_2$ [Equation (6)], the P–P distance is 2.349(2) Å, while in compound **2** a length of 2.315(2) Å is observed. The shrinking is significant and obviously due to the positive charge.

A noteworthy feature of diphosphadiboretanes (see Table 4) is that the sum of bond angles at the P atoms (average values of the two P atoms) is decreasing with increasing steric requirement of the organyl group as shown

Table 4. Selected NMR spectroscopic data of 2,4-amino-1,3-diorganyl-(silyl or hydrido)-1,3,2,4-diphophadiboretanes.

Compound	$\delta^{11}B$	$\Delta^{31}P$	B–P (Å)	B–N (Å)	B–P–B (°)	P–B–P (°)	Σ°P	Ref.
(tmpB-P*t*Bu)$_2$	63.2	4.4	1.865(2)	1.408(8)	90.1(3)	91.6(3)	339.1	
			1.876(8)	1.419(8)	8.8(3)	92.1(3)	308.5	
			1.943(8)					
			1.948(6)					
(Me$_2$NB-P*t*Bu)$_2$	50.2	–46.8	1.923(4)	1.395(5)	82.4(2)	97.6(2)	309.0	4
			1.925(4)					
(*i*Pr$_2$NB-P*t*Bu)$_2$	45.8	–48.0	1.92(1)	1.37(1)	85.0(4)	95.0(4)	313.5	6
			1.939(9)					
(Et$_2$NB-P*t*Bu)$_2$	48.9	–49.6						6
(tmpB-PCEt$_3$)	66.1	–20.0	1.916(2), 1.933(2)	1.431(2)	88.9(1)	91.1(1)	329.2	3
(tmpB-PSiMe$_3$)$_2$	60.8	–55.0	1.95(1)	1.42(1)	83.2(5)	95.9(5)	292.8	10
			1.97(1)	1.40(1)	83.5(5)	95.4(5)		
			1.95(1)					
			1.96(1)					
(tmpB-PH)$_2$	50.8	–127.2	1,913(4)	1.405(5)	89.4(2)	90.6(2)		7
			1.934(4)					
(tmpB-Pmes)$_2$	[a]	[a]	1.916(3)	1.393(3)	90.2	89.8	329.0	22

[a] No NMR spectroscopic data reported.

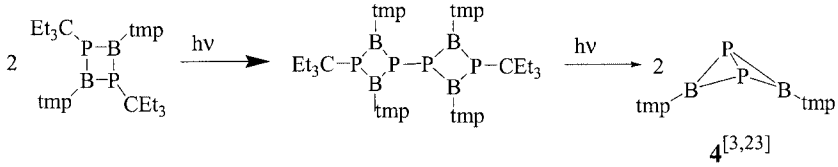

(6)

by the following data: R = CEt_3, 329.2°; R = CMe_3, 323.1°; $SiMe_3$ = 287.9°. On the other hand, in the series of compounds $(R_2NB\text{-}PtBu)_2$ this sum of bond angles decreases in the series from R_2N = tmp (332.8°) > iPr_2N (313.5°) > Me_2N (309°). Thus, the *p*-character at the P atoms increases. The result of the ring of compound **1** being nonplanar in contrast to $(tmpB\text{-}PCEt_3)_2$ is puzzling. In the latter compound the higher steric requirement of the CEt_3 group is compensated by a stronger twist of the tmp group which obviously allows ring planarity while in compound **1** the structure prefers a stronger BN bond at the expense of loss of planarity. Although the solid-state structure of **1** has two nonequivalent P atoms, in solution only one ^{31}P NMR signal is observed as well as only one each for the protons of the CMe_3 group but two ^{13}C resonances for this group. Therefore, the two P atoms are equivalent in solution.

It has been shown that $(tmpB\text{-}PCEt_3)_2$ reacts with $M(CO_5)$ fragments to yield $tmp{=}B{=}P(CEt_3)M(CO)_5$ (M = Cr, MoW).[5] In analogy, **1** reacts with $AlBr_3$ to give **3**. In contrast to compounds $tmp{=}B{=}N(tBu)EX_3$ (E = Al, Ga, In; X = Cl, Br),[17] **3** is unstable and decomposes to **2** which, however, is more conveniently obtained from **1** and $AlBr_3$ at ambient temperature followed by rapid cooling to prevent decomposition. The formation of Me_3CAlBr_2 in this process indicates that this is most likely not a radical reaction although this has not been proven definitely.

Experimental Section

All experiments were performed under anhydrous conditions using Schlenk techniques. Solvents were dried by conventional methods. $TmpBCl_2$,[23] LiPH*t*Bu,[24] and $NaN(SiMe_3)_2$[25] were prepared by literature methods. $AlBr_3$ was freshly sublimed before use. NMR: Bruker WP 200 and JEOL EX 400, IR: Nicolet FT-IR, MS: Atlas CH-7 (70 eV), X-ray: Siemens P4 four circle diffractometer operated with Mo-*Kα*-radiation, graphite monochromator, CCD detector, and the low temperature device Siemens LT2. NMR references: $SiMe_4$ for ^1H and ^{13}C; $BF_3{\cdot}OEt_2$ (ext. for ^{11}B), 1 M aqueous $HAlCl_4$ solution (ext.), 85% H_3PO_4 (ext.) for ^{31}P.

***tert*-Butylchlorophosphanyl-(2,2,6,6-tetramethylpiperidino)borane and 1,3-Di(*tert*-butyl)-2,4-(2,2,6,6-tetramethylpiperidino)-1,3,2,4-diphosphadiboretane (1):** LiPH(*t*Bu) (9.2 g, 95.8 mmol) were dissolved in diethyl ether (100 mL) – slight warming of the stirred suspension may be necessary. The clear, yellowish solution was then cooled to –60 °C, and a solution of $tmpBCl_2$, (21.2 g, 95.5 mmol) in hexane (300 mL) was added over a period of 3 h under rapid stirring. Stirring was continued overnight. After allowing the suspension to attain room temperature the orange solution was separated by a cannula from the white precipitate which was washed twice with hexane (50 mL). All solvent was evaporated in vacuo from the solution, which contained only tmpBCl–PH*t*Bu ($\delta^{11}B$ = 45.6 ppm, $\delta^{31}P$ = –52.6 ppm), leaving behind a very viscous to waxy material to which benzene (100 mL) was added. The solution was then treated with a solution of $NaN(SiMe_3)_2$ (20.9 g, 114 mmol) in benzene (200 mL). Within a few minutes a white precipitate formed. After stirring overnight the benzene was removed in vacuo and the residue treated with hexane (200 mL). According to NMR data ($\delta^{11}B$ = 63.8 ppm, $\delta^{31}P$ = 4.6 ppm) the filtrate contains only compound **1**. After reduction of the filtrate by 2/3 of its volume and cooling to –30 °C orange crystals separated within 2 d. Yield: 18.4 g of **1** (81%), m.p. 129–131 °C. ^1H NMR (C_6D_6): δ = 1.42 [t, *N* = 11 Hz, 18 H, $C(CH_3)_3$], 1.52 [m, 8 H, βCH_2], 1.61 [s, br., 16 H, γCH_2 + $C(CH_3)_2$], 1.67 [s, 12 H, $N(CH_3)_2$] ppm. ^{13}C NMR: δ = 17.1 [s, γCH_2], 32.4 [t, *N* = 6 Hz, $C(CH_3)_2$], 33.2 [t, *N* = 9 Hz, $C(CH_3)_2$], 36.1 [t, *N* = 6 Hz, $C(CH_3)_2$),], 38.6 [d, $^1J(^{31}P^{13}C)$ = 16 Hz, $C(CH_3)_3$], 54. [t, *N* = 8 Hz, $N(CH_3)_2$] ppm. ^{11}B NMR: δ = 63.8 ($h_{1/2}$ = 400 Hz) ppm. ^{31}P NMR: δ = 4.6 ($h_{1/2}$ = 90 Hz) ppm. MS: (*m*/*z*, rel. %) 421 (100), 365 (54), 316 (6), 239 (25), 224 (11), 182 (29), 126 (36), 70 (55), 57 (56). $C_{26}H_{54}B_2N_2P_2$ (478.27): calcd. C 65.29, H 11.38, N 5.86; found C 64.28, H 11.44, N 5.81

***tert*-Butylphosphinidene-2,2,6,6-tetramethylpiperidino-borane Aluminium Tribromide (3):** A solution of $AlBr_3$ (1.28 g, 4.80 mmol) in toluene (30 mL) was rapidly added to a stirred solution of compound **1** (1.12 g, 2.34 mmol, dissolved in toluene, 30 mL) at –30 °C. The mixture turned deep yellow. About 2/3 of the solvent was then removed in vacuo. From the solution, which was kept at –30 °C, golden yellow prisms separated (most of them as single crystals) within a few hours. Yield: 1.23 g, (47%), m.p. 112 °C. Additional material was retained in the filtrate including an excess of $AlBr_3$ (NMR). The compound decomposed on standing at room temperature to give an orange oil. Treatment of the oil with toluene resulted in a deep yellow solution. At –20 °C yellow crystals of **3** separated. ^1H NMR (C_6D_6): δ = 0.48, 1.40, 1.46, 1.53, 1.55 ppm. ^{13}C NMR: δ = 16.3 [s, γ-CH_2], 31.3 [s, ß-CH_2], 34.8 [d, $^2J(^{31}P^{13}C)$ = 7 Hz $C(CH_3)_3$], 37.4 [s, $N(CH_3)_2$], 57.2 [s, $C(CH_3)_2$]), 58.2 [d, $^1J(^{31}P^{13}C)$ = 8 Hz $C[CH_3)_3]$ ppm. ^{11}B NMR: δ = 68.4 ($h_{1/2}$ = 530 Hz) ppm. ^{31}P NMR: δ = –59.8 ($h_{1/2}$ = 900 Hz) ppm. MS: (*m*/*z*, rel. %) 426 (22), 411 (35), 298 (100). $C_{13}H_{27}AlBBr_3NP$ (505.85): calcd. C 30.87, H 5.38, N 2.77; found C 29.92, H 4.87, N 2.79

1-*tert*-Butyl-2,4-bis(2,2,6,6-tetramethylpiperidino)-1-phosphonia-3-phospha-2,4-dibora-bicyclo[1.1.0]butane Tetrabromoaluminate (2): A solution of $AlBr_3$ (1.0 g, 3.8 mmol) in toluene (20 mL) was slowly (1 h) added to a stirred solution of 1 (0.90 g, 1.9 mmol) in toluene (15 mL) at ambient temperature. During addition the color of the solution became light yellow. The solution was reduced in volume to about 20 mL and then stored at –20 °C. Within two weeks golden yellow crystals of **2** separated. Yield (0.2 g, 16%). Most of the crystals had single crystal quality. At room temperature the crystals turned into an oily material within a few hours. The crystals were insoluble in hexane, only slightly soluble in benzene, and dissolved in $CDCl_3$ and CD_2Cl_2 with decomposition within several minutes. ^1H NMR (CD_2Cl_2): δ = 1.41 [9 H, $^3J(^{31}P^1H)$ = 11 Hz, $C(CH_3)_3$)], 1.47, 1.56 [24 H, $N(CH_3)_2$)], 1.60, 1.61 (appr. 12 H) ppm. ^{11}B NMR: δ = 37.8 ($h_{1/2}$ = 280 Hz) ppm. ^{27}Al NMR: δ = 80.3 ($h_{1/2}$ = 50 Hz) ppm. $C_{22}H_{45}AlB_2Br_4N_2P_2$ (767.78): calcd. C 34.42, H 5.19, N 3.65; Br 41.63, found C 29.25, H 5.45, N 1.27, Br 40.9 (C and N values were always too low due to possible formation of AlN).

X-ray Structure Analysis: Single crystals were selected under perfluoro ether oil and mounted on the a glass fiber. Graphite-monochromatized Mo-*Kα* radiation was used in all cases. Compound **1** was measured on a Siemens P4 diffractometer with a scintillation counter and an LT2 low-temperature device at –80 °C in the ω/2θ mode. For compounds **2** and **3** a CCD detector was applied, and data collection was performed in the hemisphere mode.[26] For data reduction the program SAINT was used.[27] The structures were solved by direct methods implemented in SHELXTL Plus.[27] This program was also used in the refinement and SADABS for absorption correction. Non-hydrogen atoms were refined in anisotropic description, and although most H atom positions were found in the difference Fourier they were placed in calculated positions and

Table 5. Crystallographic data and data related to data collection and structure solution of compounds **1**, **2**, and **3**.

Compound	**1**	**3**	**2**
Empirical formula	$C_{26}H_{54}B_2N_2P_2$	$C_{13}H_{27}AlBBr_3NP$	$C_{22}H_{45}AlB_2Br_4N_2P_2$
Formula mass	478.27	505.85	767.78
Crystal size [mm]	0.3 × 0.3 × 0.5	0.1 × 0.2 × 0.3	0.1 × 0.1 × 0.2
Crystal system	monoclinic	monoclinic	triclinic
Space group	$P2_1/c$	$P2_1/n$	$P\bar{1}$
a [Å]	10.417(4)	8.3848(2)	10.8617(6)
b [Å]	15.482(7)	14.3300(1)	11.3177(7)
c [Å]	18.758(8)	17.5006(2)	14.7818(9)
α [°]	90.00	90.00	95.810(1)
β [°]	100.04(2)	98.04(1)	97.094(1)
γ [°]	90.00	90.00	115.114(1)
V [Å^3]	2979(2)	2082.12(6)	1608.7(2)
Z	4	4	2
ρ(calcd.), [Mg/m^3]	1.066	1.614	1.585
μ [mm^{-1}]	0.162	5.923	5.145
F(000)	1056	1000	768
Index range	$0 \le h \le 11$	$-11 \le h \le 8$	$-11 \le h \le 14$
	$0 \le k \le 17$	$-17 \le k \le 17$	$-14 \le k \le 12$
	$-21 \le l \le 21$	$-22 \le l \le 22$	$-17 \le l \le 18$
2 θ (°)	48.10	58.52	57.52
Temp. [K]	293(2)	193	193
Reflections collected	4651	12057	9046
Reflections unique	4475	3473	4862
Reflections observed (4σ)	2503	2039	3759
R(int.)	0.0585	0.0272	0.0303
Number of variables	303	188	308
Weighting scheme[a] x/y	0.0660/9.7473	0.0248/1.7484	0.0419/3.1643
GOOF	1.031	1.151	1.171
Final R(4σ)	0.0783	0.0226	0.0427
Final wR_2	0.1713	0.0537	0.0987
Largest res. peak [e/Å^3]	0.445	0.440	0.714

[a] $w^{-1} = \sigma^2 F_o^2 + (xP)^2 + yP$; $P = (F_o^2 + 2F_c^2)/3$.

incorporated into the refinement as riding on their respective C atoms. Table 5 contains the relevant information related to the crystallography, data acquisition and structure solution. CCDC-237980 to -237982 contain the supplementary crystallographic data for this paper. These data can be obtained free of charge from The Cambridge Crystallographic Data Centre via www.ccdc.cam.ac.uk/data_request/cif.

Computational Details: Geometries of the model compounds and **2** were optimized with internal redundant coordinates (total energy converged to $\le 1\times10^{-7}$ a. u., max norm of BP86/MP2/CC2 energy gradient converged to $\le1\times10^{-4}$ a. u.) with TURBOMOLE5.[29–32] using density functional (Becke–Perdew86 exchange correlation functional[33,34] for **2** and second order Møller-Plesset theory (frozen core) as well as a second-order approximated coupled cluster model for the model compounds **5**, **6**, **7** and **10** with the resolution of the identity (RI) approximation employing TZVP sets for all atoms.[35,36] For all structures, frequency calculations with SNF (MPI-parallel for **2**[37] or TURBOMOLE[38] (for the model compounds) were carried out. The geometries were re-optimized until the imaginary no imaginary frequencies remained (NIMAG = 0). NMR shift calculations were performed with the MPSHIFT module of TURBOMOLE.[39,40] ELF and AIM analyses were performed with the ToPMoD package,[41] NBO(NPA analysis with Gaussian 03 at the equilibrium geometries).[42]

Acknowledgments

We thank the University of Munich and Fonds der Chemischen Industrie as well as Chemetall GmbH for financial support. We also thank Dr. T. Seifert, and Prof. I. Krossing for recording X-ray data sets and for their help in determining the X-ray structures, Mr. P. Mayer for NMR spectra, and Mrs. D. Ewald for the MS spectra.

[1] U. Braun, T. Habereder, H. Nöth, *Eur. J. Inorg. Chem.* **2004**, 3629–3643.
[2] R. T. Paine, H. Nöth, *Chem. Rev.* **1995**, *95*, 343–379.
[3] P. Kölle, G. Linti, H. Nöth, K. Polborn, *J. Organomet. Chem.* **1988**, *355*, 7–18.
[4] P. Kölle, G. Linti, H. Nöth, G. L. Wood, C. K. Narula, R. T. Paine, *Chem. Ber.* **1988**, *121*, 871–879.
[5] G. Linti, H. Nöth, K. Polborn, R. T. Paine, *Angew. Chem.* **1990**, *102*, 715–716; *Angew. Chem. Int. Ed. Engl.* **1990**, *29*, 682–684.
[6] G. Linti, H. Nöth, R. T. Paine, *Chem. Ber.* **1993**, *126*, 875–889.
[7] M. Westerhausen, D. Dou, G. L. Wood, G. Linti, E. N. Duesler, H. Nöth, R. T. Paine, *Chem. Ber.* **1993**, *126*, 379–397.
[8] B. Kaufmann, H. Nöth, R. T. Paine, K. Polborn, M. Thomann, *Angew. Chem.***1993**, *105*, 1534–1536; *Angew. Chem. Int. Ed. Engl.* **1994**, *32*, 1446–1448.
[9] D. Dou, E. N. Duesler, R. T. Paine, H. Nöth, *J. Am. Chem. Soc.* **1992**, *114*, 9691–9692.
[10] P. Kölle, G. Linti, H. Nöth, G. L. Wood, C. K. Narula, R. T. Paine, *Chem. Ber.* **1987**, *121*, 871–876.
[11] P. Kölle, H. Nöth, R. T. Paine, *Chem. Ber.* **1986**, *119*, 2681–2685.
[12] K. Knabel, *Ph. D. Thesis*, University of Munich, **2000**.
[13] There is ambiguity about the ^{31}P chemical shifts. Therefore no data are given.
[14] S. Grundei, H. Nöth, R. T. Paine, *Chem. Ber.* **1996**, *129*, 1233–1242.

[15] J. Mason, *Multinucelar NMR*, Plenum Press, New York, London, **1987**.
[16] H. Nöth, S. Weber, *Chem. Ber.* **1985**, *118*, 2554–2556.
[17] B. Böck, U. Braun, T. Habereder, H. Nöth, *Z. Naturfosch. Teil B* **2004**, *59*, 681–684.
[18] V. Shoemaker, P. D. Stevenson, *J. Am. Chem. Soc.* **1941**, *63*, 37–40.
[19] I. Haller, R. Srivasan, *J. Chem. Phys.* **1964**, *14*, 2745–2752.
[20] B. Silvi, A. Savin, *Nature* **1994**, *371*, 683–686.
[21] H. V. Rasika Dias, P. P. Power, *J. Am. Chem. Soc.* **1989**, *111*, 144–148.
[22] A. M. Arif, A. H. Cowley, J.-G. Pakulski, M. Power, *J. Chem. Soc.Chem. Commun.* **1986**, 889–890.
[23] B. Kaufmann, H. Nöth, R. T. Paine, *Chem. Ber.* **1996**, *129*, 557–560.
[24] H. Nöth, S. Weber, *Z. Naturforsch. Teil B* **1983**, 38, 1460–1465.
[25] K. Issleib, F. Krech, M. Riemer, *Phosphorus Sulfur* **1985**, *22*, 349–352.
[26] C. Krüger, H. Niederprüm, *Inorg. Synth.* **1966**, *8*, 15–23.
[27] SMART and SAINT, Programs for data collection and data reduction, Bruker Analytical Instruments, Madison, version 5.1.
[28] SHELXTL Plus, Program for structure solution, Bruker Analytical Instruments, Madison, version 5.1.
[29] R. Ahlrichs, M. Bär, M. Häser, H. Horn, C. Kölmel, *Chem. Phys. Lett.* **1989**, *162*, 165–169.
[30] K. Eichkorn, O. Treutler, H. Öhm, M. Haeser, R. Ahlrichs, *Chem. Phys. Lett.* **1995**, *242*, 652–660.
[31] K. Eichkorn, O. Treutler, H. Öhm, M. Haeser, R. Ahlrichs, *Chem. Phys. Lett.* **1995**, *240*, 283–290.
[32] K. Eichkorn, F. Weigand, O. Treutler, R. Ahlrichs, *Theor. Chem.* **1997**, *97*, 119 –124.
[33] J. P. Perdew, *Phys. Rev. B* **1986**, *33*, 8822–8824.
[34] A. D. Becke, *Phys. Rev. A* **1988**, *38*, 3098–3100.
[35] A. Schäfer, C. Huber, R. Ahlrichs, *J. Chem. Phys.* **1994**, *100*, 5829–5835.
[36] A. Schäfer, H. Horn, R. Ahlrichs, *J. Chem. Phys.* **1992**, *97*, 2571–2577.
[37] C. Kind, M. Reiher, J. Neugebauer, B. A. Hess, *J. Comput. Chem.* **2002**, *23*, 895 –910.
[38] P. Deglmann, F. Furche, R. Ahlrichs, *Chem. Phys. Lett.* **2002**, *362*, 511–518.
[39] M. Kollwitz, J. Gauss, *Chem. Phys. Lett.* **1996**, *260*, 639–646.
[40] M. Kollwitz, M. Häser, J. Gauss, *J. Chem. Phys.* **1998**, *260*, 8295–8301.
[41] S. Noury, X. Krokidis, F. Fuster, B. Silvi, *Computers and Chemistry*, Oxford Press, **1999**, *23*, 597.
[42] M. J. Frisch, G. W. Trucks, H. B. Schlegel, G. E. Scuseria, M. A. Robb, J. R. Cheeseman, J. A. Montgomery, Jr., T. Vreven, K. N. Kudin, J. C. Burant, J. M. Millam, S. S. Iyengarm, J. Tomasi, V. Barone, B. Mennucci, M. Cossi, G. Scalmani, N. Rega, G. A. Petersen, H. Nakatsuji, M. Hada, M. Ehara, K. Toyota, R. Fukuda, J. Hasegawa, M. Ishida, T. Nakajima, Y. Hond, O. Kitao, H. Nakai, M. Klene, X. Li, J. E. Knox, H. P. Hratshian, J. B. Cross, C. Adamo, J. Jaramillo, R. Gomperts, R. E. Stratmann, O. Yazyev, A. J. Austin, R. Dammi, C. Pomelli, J. W. Ochtersi, P. Y. Ayala, K.Morokuma, G. A. Voth, P. Salvador, J. J. Dannenberg, V. G. Zakrzewski, S. Dapprich, A. D. Daniels, M. C. Strain, O. Farkas, D. K. Malick, A. D. Rabuck, K. Raghavavhari, J. B. Foresman, J. V. Ortiz, Q. Cui, A. G. Baboul, S. Clifford, J. Cioslowski, B. B. Stefanov, G. Kiu, A. Liashenkon, P. Piskorz, A. Nanayakkara, M. Challacombe, P. M. W. Gill, B. Johnson, W. Chen, M. W. Wong, C. Gonzalez, J. A. Pople, Revision B01, Gaussian Inc., Pittsburgh, PA, USA, **2003**.

Received: May 6, 2004

